COMPUTERS &
GEOSCIENCES
AN INTERNATIONAL JOURNAL

Special Issue
Benchmark problems, datasets and methodologies
for the computational geosciences
Edited by
Jef Caers

VOLUME 50   JANUARY 2013   ISSN 0098-3004

EDITORS-IN-CHIEF
JEF CAERS
STANFORD UNIVERSITY

MICHAEL PIASECKI
CITY COLLEGE OF NEW YORK

Benchmark hydrogeophysical data from a physical seismic model

Juan M. Lorenzo [a,*], David E. Smolkin [a], Christopher White [b], Shannon R. Chollett [b], Ting Sun [b]

[a] Department of Geology and Geophysics, Louisiana State University, Baton Rouge, LA 70803-4101, USA
[b] Department of Petroleum Engineering, Louisiana State University, Baton Rouge, LA 70803-4101, USA

ARTICLE INFO

ABSTRACT

Theoretical fluid flow models are used regularly to predict and analyze porous media flow but require verification against natural systems. Seismic monitoring in a controlled laboratory setting at a nominal scale of 1:1000 in the acoustic frequency range can help improve fluid flow models as well as elasto-granular models for uncompacted saturated–unsaturated soils. A mid-scale sand tank allows for many highly repeatable, yet flexible, experimental configurations with different material compositions and pump rates while still capturing phenomena such as patchy saturation, flow fingering, or layering.

The tank ($\sim 6 \times 9 \times 0.44$ m) contains a heterogeneous sand pack (1.52–1.7 phi). In a set of eight benchmark experiments the water table is raised inside the sand body at increments of ~ 0.05 m. Seismic events (vertical component) are recorded by a pseudowalkaway 64-channel accelerometer array (20 Hz–20 kHz), at 78 kS/s, in 100- scan stacks so as to optimize signal-to-noise ratio. Three screened well sites monitor water depth ($+/-3$ mm) inside the sand body. Seismic data sets in SEG Y format are publicly downloadable from the internet (http://github.com/cageo/Lorenzo-2012), in order to allow comparisons of different seismic and fluid flow analyses.

The capillary fringe does not appear to completely saturate, as expected, because the interpreted compressional-wave velocity values remain so low (< 210 m/s). Even at the highest water levels there is no large seismic impedance contrast across the top of the water table to generate a clear reflector.

Preliminary results indicate an immediate need for several additional experiments whose data sets will be added to the online database. Future benchmark data sets will grow with a control data set to show conditions in the sand body before water levels rise, and a surface 3D data set. In later experiments, buried sensors will help reduce seismic attenuation effects and in-situ saturation sensors will provide calibration values.

1. Introduction

Theoretical fluid flow models are commonly used to predict and analyze porous media flow but require verification against natural systems. Modeling approaches include pore network, lattice gas and lattice Boltzmann methods, Monte Carlo and particle methods (molecular dynamics, dissipative particle dynamics, and smoothed particle hydrodynamics), and conventional grid-based computational fluid dynamics coupled with interface tracking and a contact angle (Meakin and Tartakovsky, 2009). Although these methods are well-accepted and can achieve correct results if used with care, even the best fluid-flow simulators require assumptions and have limitations. These models remain prone to error, especially if the problems under consideration are nonlinear or have spatial heterogeneity. One way to

check model accuracy is by comparison to observed natural responses.

Classically, the water table is a saturated surface at atmospheric pressure (Deming, 2002) (Fig. 1). Another saturated surface, such as the top of the capillary fringe, can exist at lower pressures. A water-saturated medium implies 100% of the pore fluid is water, but in the near-surface and under dynamic conditions, some amount of soil gas may be retained or generated in situ. For example, some organic-rich soils can have more than 80% of their volume constituted by fluids (Nyman et al., 1990) of which at least 5% is free gas (Parsekian et al., 2012). The capillary fringe is broadly defined as being fully saturated (Lu and Likos, 2004), and the thickness of the fringe is related to the air-entry pressure (Lu and Likos, 2004) or the point at which air can enter the largest pores in the soil. For medium sand, the capillary fringe is a little less than half the height of total capillary rise (Malik et al., 1989). Capillary forces create a zone above the water table (Fig. 1) occupied by fluid moving from the water table up to a height primarily dependent on the radius of the pore throats. A system containing various pore throat sizes will likely induce "fingers" of high fluid-saturation, creating heterogeneities.

* Corresponding author. Tel.: +1 225 578 4249; fax: +1 225 578 2302.
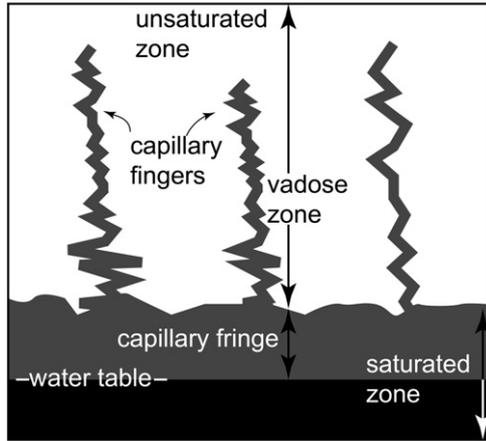E-mail address: gllore@lsu.edu (J.M. Lorenzo).

Fig. 1. Soil saturation zones. At least three different saturation levels between water table and surface (adapted from Lu and Likos, 2004 and Deming, 2002) are expected for shallow loose soils. A fully saturated zone lies below the water table (black). Pore pressure at water table is atmospheric. Above the water table lies a second saturated zone (gray zone) where pore pressure is less than atmospheric. Unsaturated conditions (white zone) prevail where air can enter pore spaces. Irregular unconnected capillary fingers are able to reach the top of the capillary fringe.

Additionally, whenever water levels drop, whether due to natural causes or pumping, some water remains trapped in the pores due to capillary forces. The trapped water creates a residual saturation and forms the vadose zone between the surface and the water table.

Large-scale field projects and reference sites (e.g., Koch et al., 2009) are capable of providing data with which to test constitutive flow models, but they can be costly, in time and money. Resultant data can be sparse and may require careful geostatistical characterization especially in heterogeneous sediment (Barrash and Clemo, 2002). Even homogeneous field sites can be constrained by weather and tides (Bachrach and Nur, 1998a). Moreover, because models of large natural systems can be limited (Oreskes et al., 2007) a lab-scale experiment may help complement our understanding of these models.

Fully described experimental data sets, publicly available on the internet, provide benchmark cases to which flow simulations and soil physics models can be compared. Mid-size experiments can be controlled and modified while maintaining complexity in the physical characteristics of the media. Herein, we focus on a seismic laboratory experiment and present eight data sets plus the details of their collection. Preliminary analyses of these initial results imply additional experiments are needed; their data will also be made public. We refer to this work collectively as the sand tank experiment. The sand tank serves as an unconfined model reservoir or aquifer, and because seismology can be used to image features on multiple scales, it lends itself to physical modeling.

Such open-source data can provide a readily available, common-reference and inexpensive body of observations that multiple researchers can use to test granular soil and fluid flow models. We envision future expansions of these data sets to include useful parameters such as water-level pressure, temperature and in-situ measured saturation that can help calibrate models. Additional sand tank experiments can incorporate lowering as well as raising of water levels in order to capture hysteretic effects, which have been observed seismically (Knight and Nolen-Hoeksema, 1990).

Seismic detection of subsurface water saturation remains a challenge to near-surface seismology. Seismic experiments conducted during pumping tests generally are able to detect amplitude changes in reflection events attributed to an increase of the zone of heterogeneous partial saturation (Birkelo et al., 1987; Sloan et al., 2007) and an increase in complexity. Yet, the ability to measure the changes in the height of the water table from the surface, or its proxy, can provide information on aquifer properties (Birkelo et al., 1987), soil conditions in agriculture, and contaminant flow and removal. While electromagnetic methods have been in common use for many years (e.g., Neill, 1990; Zhody et al., 1974) and are considered essential in groundwater investigations (Santamarina et al., 2005), in their absence seismic parameters such as V_P/V_S (compressional wave velocity/shear wave velocity) ratios can be used as good indicators of variations in fluid saturation (Grelle and Guadagno, 2009).

The strongest seismic reflections are expected to emanate across the largest changes in acoustic impedance (seismic velocity times density), possibly corresponding to the top of the saturated capillary fringe (Fig. 1). However, even in the case of a nominally homogeneous medium, heterogeneity in the acoustic impedance can also be affected by factors such as matric suction (Hicher and Chang, 2008), or patchy saturation (Knight et al., 1998; Konyai et al., 2009). The capillary electro-attractive force between the water and solid grain surfaces and the origin of matric suction is strongly dependent on the size of the pore throats and the angle of the wetting fluid (Deming, 2002). Patchy saturation can have a significant impact on seismic velocities. The size of the patches relative to the wavelengths used (Knight et al., 1998) can provide an inaccurate image of the subsurface. Relatively controlled geological homogeneity, as in our sand tank, can minimize the effects of patchy saturation and can create a system that is more easily imaged by seismological methods.

Often, predictions of seismic velocities in saturated–unsaturated unconsolidated sediments require an estimate of the effective values of the wet bulk (K_{wet}), wet shear moduli (G_{wet}) and wet bulk density (ρ_{wet}) of the medium where

$$V_P = \sqrt{\frac{K_{wet} + \frac{4}{3}G_{wet}}{\rho_{wet}}} \text{ and } V_S = \sqrt{\frac{G_{wet}}{\rho_{wet}}}$$

At the low-frequency limit in Gassman–Biot theory (Gassmann, 1951; Biot, 1956) K_{wet} is relatable to the reference bulk modulus of the framework of mineral grains (K_{ref}) whose porosity is ϕ, the bulk modulus of the minerals comprising the sediment (K_{min}), and the bulk modulus average of the pore fluid (K_{fl}), as follows (Mavko et al., 1998, p. 168):

$$\frac{K_{wet}}{K_{min}-K_{wet}} = \frac{K_{ref}}{K_{min}-K_{ref}} + \frac{K_{fl}}{\phi(K_{min}-K_{fl})}$$

and where the shear modulus (G_{ref}) is unchanged by the pore fluids. In addition, K_{ref} and G_{ref} can be provided by a generalized Hertz–Mindlin (Mindlin, 1949) contact theory extended to a randomly disordered, stack of spheres as:

$$K_{ref} = \sqrt[3]{\frac{C^2(1-\phi)^2 G_{min}^2}{18\pi^2(1-\upsilon)^2}P_{eff}}$$

$$G_{ref} = \left(\frac{5-4\upsilon}{5(2-\upsilon)}\right)\sqrt[3]{\frac{3C^2(1-\phi)^2 G_{min}^2 P_{eff}}{2\pi^2(1-\upsilon)^2}} \quad \text{(Mavko et al., 1998)}$$

where C (coordination number) is the average number of contacts between grains, G_{min} is the shear modulus and υ is Poisson's ratio of the mineral grain, and P_{eff}, the effective confining stress between grains. An increase in saturation in the sand body increases the overall bulk density and through hydrostatic buoyancy, may also decrease the effective confining stress – $P_{eff} = (\rho_{min}-\rho_{water})(1-\phi)g\,z$, (Velea et al., 2000) – both processes act to decrease the overall V_P. Modifications to the basic assumptions such as the actual smoothness of grains and direct grain contact interaction may limit the accuracy of these velocity predictions (Bachrach et al., 2000; Velea et al., 2000). Intrinsic

attenuation may result from friction between the grains due to variations in size and roundness. In a forward modeling approach, these parameters could be iteratively adjusted to best match velocity estimates and used for comparison between different localities.

2. Methods

We collect, single-, vertical-component, acceleration data in a large cement tank, (0.65-by-8.7-by-5.7-m in size) filled with a flat-topped body of sand ∼0.44+/−0.01 m thick (Fig. 2) that serves as an unconfined aquifer or reservoir. The bottom of the sand tank is not perfectly flat and appears to vary by ± 0.01 m. The sand body thickness is 0.44 m along the northern two meters of the tank and then gradually thins to the south to 0 m at 4 m from the northern end of the tank. Three observation wells are used to measure free water levels (Fig. 2). Wells are held open with .0508 m diameter PVC pipes that are machine slotted, or screened, over the whole well at "10 slot" (∼2.54 × 10^{-4} m slits). Slit dimensions are chosen to allow water flow into the well but exclude the sand (Wentworth, 1922). The sand tank contains two layers of well-sorted, medium-grained sand (Table 1 and 2). The thickness of the two layers is variable throughout the tank. In the thinner parts of the sand body, the bottom layer is ∼0.02 m thick and the upper layer is ∼0.12 m. Where the sand body is thickest, the lower layer is much thicker, ∼0.31 m, and the upper layer is ∼0.13 m thick.

The dual-layer system can create the potential problem of an early reflector (Sherlock and Evans, 2001). However, as the sand tank is used in other ongoing experiments it cannot be homogenized. A few small objects, such as small pockets of clay and sea shells, also occur in the sand tank. Two clay pockets found are as much as 0.04–0.05 m wide and up to 0.005 m thick and could cause diffractions. The three shells, measuring between about 0.03–0.06 m wide and 0.01 m thick, are also potential diffractors. As long as grains are smaller than about an eighth of the wavelength, they should not cause diffractions (Sherlock and Evans, 2001), and we can consider the average elastic moduli to

characterize the medium. Although our sensors are ∼0.01 by 0.01 m in their largest dimensions and near the limit of seismic resolution, we do not observe the diffractions from the shells.

The sand tank is first fully filled and then drained 24 h prior to data acquisition in order to improve coupling between the sensors and the sand. Sensors are buried 0.01 m below the top of the sand, and the effective source depth is taken as 0.02 m. Each experiment is assigned a label of the form "WL1", which stands for water level 1. In the first experiment, "WL1", the water level depth lies ∼0.01 m above the base of the sand tank. Water

Table 1
The sand tank contains two layers of well-sorted, medium-grained sand (Wentworth, 1922). For the grain size distribution in the upper and lower sand, grain-size diameter (mm)=2^{-phi}.

Upper sand	Mean (phi)	Mean (mm)	Sorting	Skewness	Kurtosis
Sample 1	1.39	0.380 mm	0.47	0.029	0.874
Sample 2	1.19	0.438	0.38	0.197	1.028
Sample 3	1.55	0.341	0.47	−0.205	0.965
Lower sand					
Sample 4	1.71	0.305	0.43	−0.023	1.029
Sample 5	1.71	0.305	0.43	−0.017	1.032
Sample 6	1.69	0.309	0.47	−0.025	1.068

Table 2
Water elevation values at different sand tank locations over a ∼2-day period.

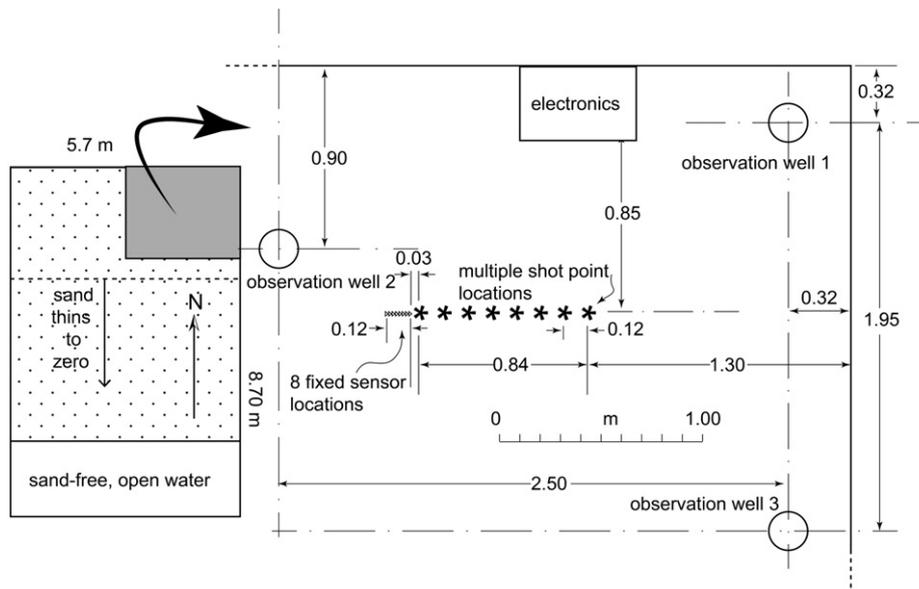|	Open water	Well 1	Well 2	Well 3	Average	Time
WL1	11.2	9.4	9.2	11	9.9	(DAY1) 10:35 p.m.
WL2	16	14.3	14.3	15.7	14.8	(DAY2) 3:05 p.m.
WL3	20.5	19	19.4	20.3	19.6	7:02 p.m.
WL4	26	24.6	24.9	25.8	25.1	10:00 p.m.
WL5	31	29.8	29.6	30.6	30	11:10 p.m.
WL6	38	36.8	37	37.5	37.1	(DAY3) 1:38 a.m.
WL7	40	39	39	40	39.4	2:01 a.m.
WL8	43	43	43	43	43	2:23 a.m.

Fig. 2. Map layout of seismic acquisition equipment and observation wells in sand tank. Pseudowalkaway experiment is set up in a 0.44 m thick section of sand at least 0.85 m away from nearest wall in an east-west orientation, which should provide a constant stress direction as water level varies. Sand surface is leveled prior to data acquisition. Eight sensors are buried 0.01 m below surface of sand to improve coupling and are placed ∼0.017 m apart, center-to-center, leaving < 0.002 m of sand between each sensor, for a total center-to-center array length of 0.12 m. First shot point is 0.03 m east of sensor array and each subsequent shot location is moved 0.12 ± .005 m for a total of eight shots points (asterisks) and a maximum offset of ∼0.99 m. Location errors are estimated at 10% of numbers shown.

Table 3
Source and sensor equipment and software requirements, and seismic acquisition parameters used in this paper.

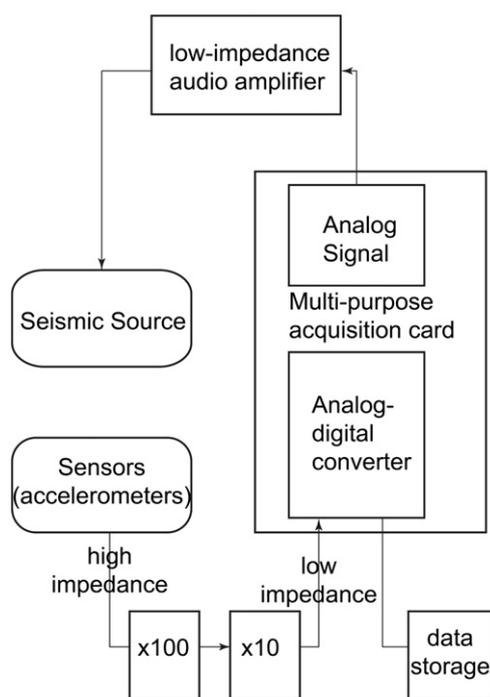| Seismic sensor	
Sensor characteristics	Piezo-electric accelerometer of polyvinylidene fluoride film composition (ACH-01from Measurement Specialties Inc.); nominally flat response of ~9 mV/g +/−1 mV, response over 20 Hz–20 kHz frequency range.
Stage 1 signal conditioning	100-fold operational amplifier (LT1115 from Linear Technologies) (Fig. 4).
Stage 2 signal conditioning	10-fold audio amplifier, (DI800, from Behringer) converts single-ended signal to differential. Output low impedance (680 Ω), matches required input impedance for analog-to-digital acquisition card.
Pseudo-array dimensions	64 sensors, 0.03 m–0.99 m source-receiver offsets, ~0.017 m sensor spacing (Fig. 2).
Recording electronics	
Multi-purpose digital acquisition card	Onboard, PCI-based analog-to-digital acquisition (AD) card with an 8 differential-channel mode input (Model PCI-6251 from National Instruments, Inc.) software triggering, and low-impedance analog output for source wavelet.
Instrument control software	Modified version of multi-function-synch AI–AO.vi written in "G", a commercial virtual instrument software programming language (from National Instruments).
Sample rate	72 kS/s, per analog-input differential channel (8)—maximum possible of 156.25 kS/s.
Nyquist frequency	36 kHz.
Input and output voltage resolution	1 in 16 bits; 305 μV (+5%) for a +/−10V range.
Acquisition format	LabView© (National Instruments) ASCII format converted to SEG Y (Barry et al., 1975) using seg2segy (Sioseis, 2011). SEG Y data records for each sensor have 13 μs sample intervals and contain 780 samples.
Seismic source	
Source wavelet	Ricker wavelet, central frequency at 10 kHz, 23 samples at 50 kS/s, 50 μs wide side-lobes; synthesized digitally by PCI-6251 AD card.
Seismic source generator	Magnetostrictive ultrasonic transducer (Model CU-18 from Etrema Products Inc.). Low-impedance audio amplifier (Model RMX 2450 from QSC Audio Products LLC) amplifies input Ricker source wavelet to drive this transducer at +150 V (max); Shots (8) are spaced ~0.12 m apart (Fig. 2).
Seismic software filtering, manipulation and display	Seismic Unix Processing System (Stockwell, 1999).

Fig. 3. Schematic signal flow sequence between seismic source generation and seismic monitoring of experiment (Table 3).

Fig. 4. Simplified electronic diagram. First-stage amplifier (Table 3; Fig. 3) with 100-fold amplification.

enters the tank from a spout on its southern end into open water, lateral to the main body of sand. Water levels are successively increased in ~0.05 m increments until they reach stage "WL8", ~0.01 m from the top of the sand. At the start of the first experiment it is not feasible to eliminate all water in the pores of the sand because the sand body is too large to dry by traditional methods (baking) and capillary forces tend to hold on to the fluid for very long periods of time. Incomplete saturation is always observed in the sand tank in the form of air bubbles that are released when the sand is disturbed.
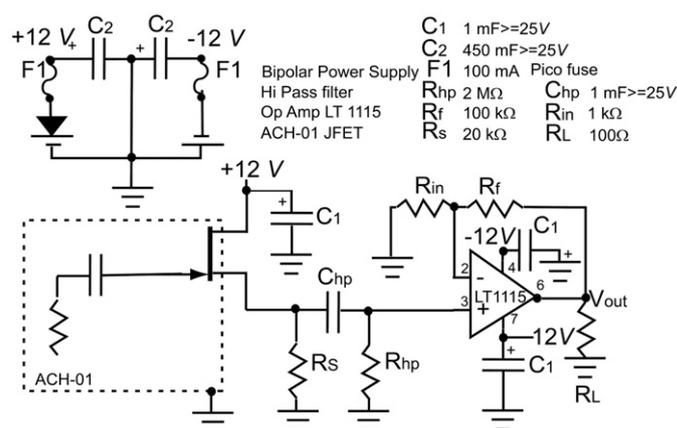
Data are collected using a pseudowalkaway geometry (Vincent et al., 2005) that uses a fixed array of 8 accelerometers (Table 3) and eight off-end, shot-points (Fig. 2) collinearly transposed (Evans, 1997). Nominally, a shot-point spacing equal to the geophone spread length provides laterally continuous, but non-overlapping subsurface seismic returns while expediting data acquisition. Lateral subsurface heterogeneities could cause small time shifts between subarrays but these prove manageable for estimating seismic velocities in our data. Care is taken in lining up the survey sensors and sources although inconsistent separations can also induce small time shifts in the data. We can attempt to quantify the worse-case timing errors that can arise from incorrect placement of each sensor within the loose sand. When observed, the sign of the shifts is normally monotonic, moves the data to later times and has a maximum cumulative total shift of ~0.5 ms over all 64 traces. In other words, when linearly distributed throughout, there could be ~8 μs (downward) in timing error per trace if all the shift is attributed to experimental error. Interpreted V_p values could increase by ~10%, although the differences between V_P-models derived from different water-level

experiments would change by a smaller amount. We note that because we are attempting to evaluate the usefulness of the seismic technique, we have not collected CDP-type profiles but individual pseudowalkaway noise tests.

Each shot-gather was formed from the sum of 10–100 repeated scans through a sensor array (Fig. 3). It is expected that summed gathers increase the signal-to-noise ratio; assuming random noise sources. Unsaturated and unconsolidated sand as a modeling

material severely attenuates signal and has a low quality factor in the range of 3–10 (Jongmans, 1990; Prasad and Meissner, 1992). A stacking of 10-to-100-fold is found to recover useful data. Normally the travel distances in our sand body are less than 1 m.

Special care was used to reduce sources of instrument noise. Accelerometers were wrapped in grounded copper foil to shield against 60 Hz noise, and sealed with liquid electrical tape to protect against moisture. Best coupling between sensors and the
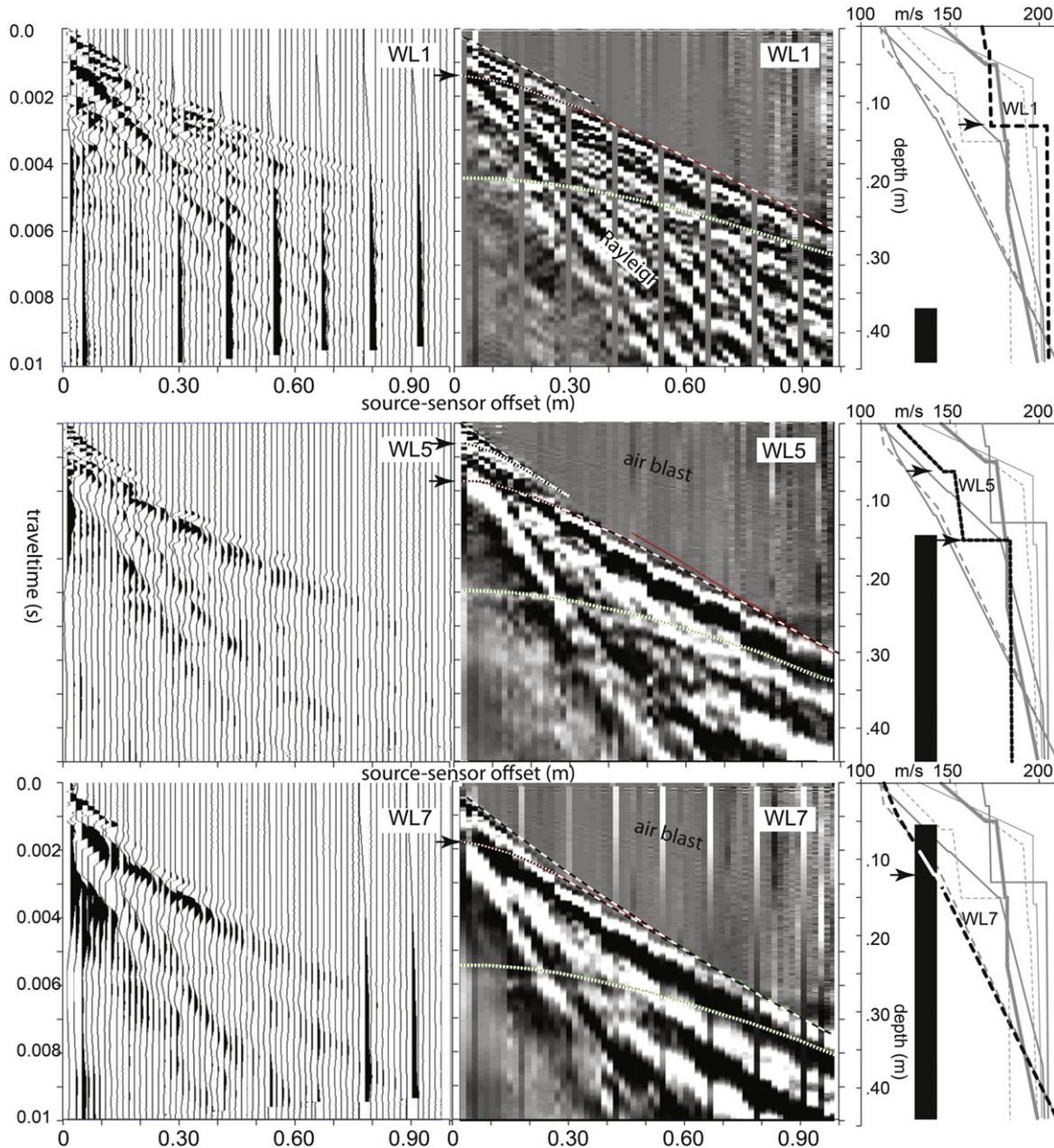

Fig. 5. Representative seismic data sets. Three seismic data sets (experiments "WL1", "WL5", "WL7" out of 8 total) recorded at different water levels (black bar and Table 3) each displayed with two different formats. Boundary between the two sand types lies at depth of 0.13 ± 0.01 m. On left, uninterpreted, variable-area wiggle plots represent positive seismic data amplitudes in black. Amplitudes are rebalanced through division by root-mean-square average, but otherwise are shown unfiltered as in raw data available online. Left-panels "WL1" and "WL7" show long-period electronic noise in one accelerometer, but because pseudowalkaway geometry employed in experiment uses only eight fixed sensors, for all 8 sources, noisy trace reappears at intervals of 8 traces. Noisy traces can be suppressed readily by high-pass filtering. On right panels, same data are shown interpolated among variable shades of gray but with noisy traces removed. Synthetic seismic events, forward-modeled using rays (dashed lines) are drawn over raw seismic panel. V_P–depth models (Figure 6), used to calculate distance-traveltime locations for seismic rays are shown highlighted with bold lines in V_P–depth panels to far right of each data set. Principal identified seismic events in data, lie parallel and below calculated synthetic events. Reflected synthetic events are convex-downward (short dashes) and refracted synthetic events (long dashes) have a straight or slightly concave-upward shape. Horizontal arrows match reflector events in seismic data to velocity jumps in V_P–depth models. Faint, early linear arrival across whole panel is interpreted to correspond to ground-coupled air-blast. Surface (Rayleigh) waves tend to arrive at same time as early reflections. Surface waves are a major cause of noise for interpreting possible shallow reflector events. However, slope filtering (frequency-wavenumber) of these arrivals neither revealed any underlying strong reflectors, nor improved their quality significantly.

sand was achieved by burying the sensors at about 0.01 m depth below the sand top. The center of the seismic source lay effectively at a depth of ~0.02 m. Amplifying boxes are metallic and grounded (Fig. 4). Signal wires between the amplifier and the digitization card used differential connections and all wires were electrically shielded. Seismic data from each experiment remain unfiltered in the public data sets and are gained (Stockwell, 1999) only for display purposes (Fig. 5).

Controlled-source seismic experiments in the field investigating the natural water table involve dominant central frequencies that range from about 100 Hz to 1000 Hz (Bachrach and Nur, 1998a; Sloan et al., 2007). In the sand tank, where V_P is of order 10^2 m/s and the dominant frequency is ~2.5 kHz, if we use a half-wavelength criterion, the vertical seismic resolution is 10^{-2} m. During a test of the seismic sensor array, amplifiers and recording system (Figs. 3 and 4) (Smolkin, 2011) and before the water level began to rise in the sand body, V_P at the surface in the upper sand unit, was determined to be ~150 m/ increasing to ~200 m/s at a depth of 0.07 m. For this purpose, a wooden board (.32 × .14 × 0.05 m) was buried in the sand at a depth of 0.07 m in a section of the sand tank where total sand thickness is 0.15 m, at the southern toe of the sand wedge. At the scale of our experiment we have detected only one set of P-waves, and only low-frequency Biot Theory (Biot, 1956) is considered. We employ average bulk densities, the shear and incompressibility moduli of the combined body of sand and water mix, and assume that at our scale the effects of individual sand grains are not influential.

3. Data format

Acquired seismic data are stored initially in a commercial Lab-VIEW© (National Instruments, 2009) format (".lvm"). The ".lvm" data format is a text based, tab delimited format, which is easy to manipulate with scripts created in programming languages such as Perl. The ".lvm" files include metadata such as the date and time, the sample rate, the number of channels, and the number of samples for each acquisition. We employ Perl scripts to convert ASCII files into a widely used standard seismic exchange format known as SEG Y (Barry et al., 1975). Within each SEG-Y data file, data traces are preceded by a 240-byte-long binary header that contains a sequential number for each accelerometer (lower numbers are closer to source), sample numbers, sample rate and numbers of samples. All 8 water-level experiments can be downloaded from http://github.com/cageo/Lorenzo-2012.

4. Analysis and results

All data sets display at least 2–3 key seismic reflector- and refractor-events (Fig. 5) whose shape we attempt to best-match by forward-tracing rays (Cerveny, 2001) through a simple, one-dimensional V_P-depth model that uses either constant-velocity and/or gradient-velocity layers (Figs. 5 and 6). These interpretations should be viewed as a starting reference for later workers. Surface waves (predominantly interpreted as Rayleigh waves) tend to overlap and obscure the earliest reflections and are not yet considered in these models.

The earliest visible arrivals correspond to a refractor whose concave-upward shape and lateral extent is best matched by a linear velocity gradient. Concomitant with the rise in water level, the deepest/latest visible event in the data moves to later arrival times (from 4.5 ms to > 5 ms), and is most easily matched by an overall consistent velocity gradient from the top to the base of the sand body (~110–210 m/s, e.g., in case "WL8"). As well, a large step in the V_P-depth models (e.g.,~160–180 m/s in case "WL5") is no
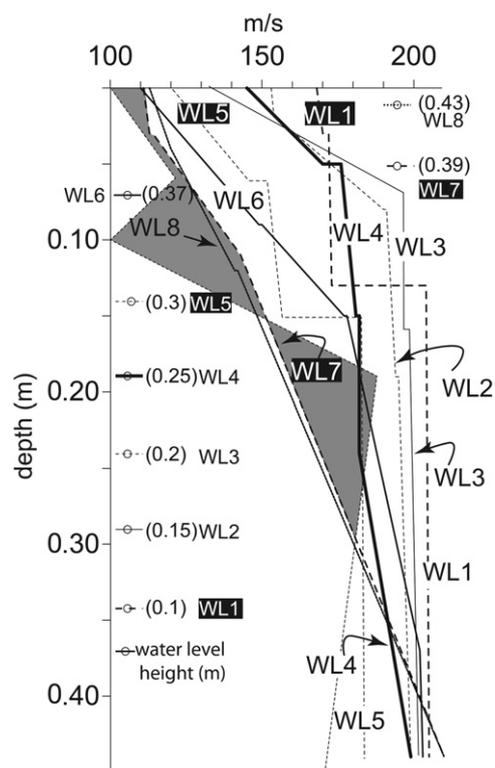

Fig. 6. V_P-versus-depth models. Eight (WL1 through 8) V_P-versus-depth models derived from time-offset ray-tracing of principal refraction and reflection events (Fig. 5) each collected at eight different water levels measured from the bottom of the sand tank (Table 2 and values along left margin and top right corner). Largest velocity changes occur in uppermost section and smallest changes at base of sand body. Rayleigh wave velocity values also appear to decrease as water levels rise. Smallest apparent Rayleigh wave velocity in WL1 (0.01 m water level) is 65 m/s ± 10 % and decreases to 55 m/s ± 10 % in WL7 at a higher water level (0.39 m). An alternative V_P-depth model (Smolkin, 2011) that uses low-velocity zones to best match arrivals is shown with dashed line. Gray polygons highlight difference between the alternative model and the V_P-depth model for case WL7.

longer required for case "WL7". This velocity step is more prominent for data cases where water is shallower and appears at a depth (~ 0.12–0.15 m) similar to that of the base of the first sand layer.

Several first-order trends in the interpreted V_P—depth models attend the increase in water levels. Minimum velocity values in the near-surface of the sand decrease from ~175 m/s to ~100 m/s, (40% decrease) whereas the deepest maximum velocity value of ~210 m/s decreases substantially less (~15%), thereby increasing the average velocity gradient and arrival times of the deepest reflector. A strong reflector in each shot gather is interpreted to correspond to the hard bottom of the tank at the base of the sand. Frequency content also decreases with increasing water levels. Instantaneous frequency content of the refracted events appears to decrease from a dominant value of 2.7 kHz to 2.4 kHz. The frequency content of the reflections is difficult to determine because of the data quality, although they appear to be higher frequency than the refractions.

We interpret that the deepest reflector corresponds to the bottom of the sand tank and so hold the maximum depth in our models at ~0.44 (+/−.01 m). Also, most of the experiments show a possible shallow reflector boundary at 0.10–0.15 m below the top of the sand (Figs. 5 and 6) that may correspond to the two sand layers detected through grain-size analysis. A less-defined layer boundary exists between 0.05 m and 0.1 m depth that can be interpreted as a change in velocity gradients (WL 2,4 and 5) However, saturation must be more than 99 percent for the overall stiffness to be high enough to increase the V_P to an order 10^3 m/s.

5. Discussion

The very preliminary nature of the results above indicates an immediate need for several additional experiments whose data sets will be added to the online database.

(1) A future data set will include a control experiment to establish the initial conditions of the sand pack before the tank is filled with water.

(2) The relation between seismic velocity and saturation through contact theory (Mindlin, 1949) and Biot–Gassman (Gassmann (1951)) substitution equations can be directly validated with in-situ saturation measurements. Five new saturation sensors are currently being incorporated into the sand tank and will be used to grow the open benchmark data set.

Unless saturated conditions of more than 99% are met (Bachrach and Nur, 1998a), V_P values are expected to be of the order 10^2 m/s, similar to those observed in the sand tank A lack of complete saturation in the sand at even the highest water levels means there is no large seismic impedance contrast across the top of the water table to generate a clear reflector. Most probably there is always a small undetermined percentage of irreducible water that never permits fully dry conditions in these experiments, even when the sand is completely covered by a layer of water. As such, at the time scales observed in these experiments ($\sim 10^5$ s) the capillary fringe does not, as expected, appear to completely saturate because the interpreted velocity values remain so low. Even in marine settings, a small amount of gas ($\sim 1\%$ of overall porosity) can keep V_P in the same range 10^2 m/s (Anderson and Hampton, 1980).

We observe that as water levels increase, the deepest reflector in the seismic data, (base of the tank) appears at later times and there is an overall decrease in V_P values. When combined with the Gassmann (1951) fluid substitution equation, a modified contact theory can help explain an almost 10% decrease in V_P and V_S (Bachrach et al., 1998b, 2000). Otherwise, only with very dry sand do Hertz–Mindlin equations (Mavko et al., 1998) predict low values V_P (e.g., less than 100 m/s) especially at shallow depths (less than 0.01 m),where the overburden pressure is small.

(3) In the sand tank, complete uniformity in grain packing cannot be guaranteed and some degree of heterogeneity is probably introduced, although far less than would be expected under normal field conditions. Capillary fingers as well as zones of variable permeability can create patchy saturation and contribute to changes in heterogeneity as water levels rise during the different experiments. Fingering and patchy saturation can generate three-dimensional effects, which the line of sensors in the sand tank cannot readily detect. The sand tank has been recently supplemented with 48 sensors and two additional mechanical vibrating sources for greater surface coverage. When used in orthogonal groups of three, the sensors are capable of acting as three-component accelerometers. Future sand tank data set will include a grid of surface sensors and attempt to generate a 3D-vetical component seismic data set. Patchy saturation can be of great concern if patches are of a size comparable to the wavelength. The 10^{-2} m wavelengths in the upper parts of the tank can induce low and high velocity zones within the data, which could be observed as non-systematic discontinuities in the refracted events. Let us take the simple case of a "patch" of saturation 0.01 m wide characterized by $V_P=150$ m/s embedded in a higher velocity medium (200 m/s) of total width 0.1 m. A patch that spans 10% of the total transmission distance could add $\sim 1.6 \times 10^{-5}$ s to the total traveltime. Time shifts ($\sim 6 \times 10^{-5}$ s)

between adjacent shot gathers of comparable lateral extent, are observable in the pseudowalkaway data sets and could contain possible contributions from patchy saturation.

(4) An experimental geometry consisting of buried geophones and surface sources has the advantage of reducing seismic attenuation (e.g., Velea et al., 2000). A combined array of surface and sensors down a well in the sand will be possible with the enlarged sensor array.

(5) Repeated episodes of filling and draining may be useful for evaluating possible hysteretic effects in the unsaturated zone. As well, spatial changes in saturation (e.g., Knight and Nolen-Hoeksema, 1990) between experiments, may be addressed.

Two remaining, but possibly less-significant processes, could also change V_P values in the sand tank data. Decreasing capillary forces can lower contact pressures between grains, and may reduce observed velocities (Bachrach et al., 1998b). An increase in temperature can also reduce V_p. In our experiment, the measured inflowing water temperature was 19° C while room temperature was held at 21° C. An increase of ~ 4 °C can decrease $V_P \sim 30$ m/s (Velea et al., 2000) especially in zones of greatest saturation. We expect temperature effects to be minimal near the surface (0–0.01 m) during the first experiments when water levels (WL1, WL2) are low. In addition, the experiment lasted ~ 2 day which allowed for a considerable degree of thermal equilibration.

The large size of the sand tank is advantageous because we can place sensors far enough from its edge so that the wall effects can be disregarded. Edge-effect reflections arrive late enough that they do not affect primary arrivals. In smaller experiments (~ 1 m diameter tank; Velea et al., 2000) friction against adjacent container walls also reduces V_P by lowering grain-to-grain contact stresses.

Various sources of error can contribute to variations in the V_P-depth models and should be considered by workers when modeling the data provided. Interpreter error can accompany V_P-depth model estimates. Through trial and error we find that V_P in our models can vary ~ 2–10% of the final value and continue to match near and far-offset seismic events within the 1/4 of a wavelet of the selected arrival time. Similarly, modeled depths for each seismic arrival are limited to within $+/-0.01$ m.

Alternative interpretations of refracted arrivals are possible. For example, Smolkin (2011) interprets the top of a low-velocity zone at depths of 0.06–0.09 m in order to explain the sharp decreases in refracted amplitudes beyond distances of 0.2 m from the source (Fig. 5). Overall, V_P values are comparable and a shallow low-velocity zone appears compensated by deeper higher velocities (Fig. 6), probably in order to match the same overall refraction arrival travel times. Partial saturation can create a low-velocity layer which makes seismic refraction data difficult to interpret (Bachrach and Nur, 1998a; Bachrach et al., 1998b). Unless confirmed independently, such as by the presence of phase reversals from reflection events at the top of the low-velocity layer, additional data analysis may be needed. Dispersion analysis of surface waves (Socco and Strobbia, 2004) contained in the available data sets can test this hypothesis and provide shear-wave velocity (V_S) profiles. Together, V_p/V_S ratios have been proposed as more sensitive to saturation than V_P alone (Grelle and Guadagno, 2009)

6. Conclusions

A large sand tank at a 10^{-2}–10^{-3} scale of field conditions creates a modeling environment that is safe, controllable, and without hydraulic or seismic edge effects. Eight two-dimensional seismic data sets sample the sand body as water levels are raised

at a constant increment starting at 0.01 m and ending at 0.43 m, or 0.01 m below the top of the sand. A repeatable seismic source produces dominant frequency centered on 2.5 kHz, which provide a vertical resolution of 10^{-2} m. Source-receiver offsets range from 0.03 m to 0.99 m, more than double the maximum thickness of the sand body. At these relatively low frequencies, a modified granular contact theory (Velea et al., 2000) together with Gassmann (1951) fluid substitution con only partly explain the observed overall decrease of V_P with increasing water levels.

Preliminary results suggest a need for several additional experiments whose data sets will be added to the online database. Future experiments envisage generation of a control data set prior to the start of experimentation. An increase in the number of accelerometers from 8 to 48 and two additional mechanical vibratory sensors will permit denser sampling of the subsurface in order to detect saturation-caused heterogeneities. In later experiments, buried sensors will help reduce seismic attenuation effects and new saturation sensors values will complement the data set.

Refraction and reflection seismic events are best-matched by ray-tracing to generate estimates of V_P versus depth (estimated errors of 2–10%) for each experiment. A dominant trend derived from these interpretations is that rising water levels reduce near-surface V_P values while increasing the overall gradient in V_P-depth trend. Maximum V_P values at the bottom of the sand body remain less than 210 m/s and suggest that saturation conditions remain below near-full saturation. Water saturation appears to reduce the contrast in V_P across several interpreted layer boundaries. There is also some residual saturation in the sand pack even when the tank is completely drained.

All data sets are available for public downloading in a standard seismic SEG Y format (Barry et al., 1975). These open-source data can provide common-reference observations that other workers can use to test and improve granular soil and fluid flow models. As with field data, our data carry inherent uncertainties in the degree of heterogeneity of saturation distribution.

Acknowledgements

References

Anderson, A.L., Hampton, L.D., 1980. Acoustics of gas-bearing sediments II. Measurements and models. Journal of the Acoustical Society of America 67, 1890–1903.

Bachrach, R., Nur, A., 1998a. High-resolution shallow-seismic experiments in sand, Part I: Water table, fluid flow, and saturation. Geophysics 63, 1225–1233.

Bachrach, R., Dvorkin, J., Nur, A., 1998b. High-resolution shallow-seismic experiments in sand, Part II: Velocities in shallow unconsolidated sand. Geophysics 63, 1234–1240.

Bachrach, R., Dvorkin, J., Nur, A.M., 2000. Seismic velocities and Poisson's ratio of shallow unconsolidated sands. Geophysics 65, 559–564.

Barrash, W., Clemo, T., 2002. Hierarchical geostatistics and multifacies systems: Boise Hydrogeophysical Research Site, Boise, Idaho. Water Resources Research 38, 18.

Barry, K.M., Cavers, D.A., Kneale, C.W., 1975. Report on recommended standards for digital tape formats. Geophysics 40, 344–352.

Biot, M.A., 1956. Theory of propagation of elastic waves in fluid saturated porous solid. I. Low frequency range. Journal of the Acoustical Society of America 28, 168–191.

Birkelo, B.A., Steeples, D.W., Miller, R.D., Sophocleous, M., 1987. Seismic reflection study of a shallow aquifer during a pumping test. Ground Water 25, 703–709.

Cerveny, V., 2001. Seismic Ray Theory. Cambridge University Press.

Deming, D., 2002. Introduction to Hydrogeology. McGraw-Hill Companies, Inc, New York 480 pp.

Evans, B.J., 1997. A Handbook for Seismic Data Acquisition in Exploration. Society of Exploration Geophysics, Tulsa.

Gassmann, F., 1951. Uber die elastizitat poroser median. Vierteljahrsschrift der Naturforschenden Gesellschaft in Zürich 96, 1–23.

Grelle, G., Guadagno, F.M., 2009. Seismic refraction methodology for groundwater level determination: "Water seismic index". Journal of Applied Geophysics 68, 301–320.

Hicher, P.Y., Chang, C.S., 2008. Elastic model for partially saturated granular materials. Journal of Engineering Mechanics 134, 505–513.

Jongmans, D., 1990. In-situ attenuation measurements in soils. Engineering Geology 29, 99–118.

Knight, R., Dvorkin, J., Nur, A., 1998. Acoustic signatures of partial saturation. Geophysics 63, 132–138.

Knight, R., Nolen-Hoeksema, R., 1990. A laboratory study of the dependence of elastic wave velocities on pore scale fluid distribution. Geophysical Research Letters 17, 1529–1532.

Koch, K., Wenninger, J., Uhlenbrook, S., Bonell, M., 2009. Joint interpretation of hydrological and geophysical data: electrical resistivity tomography results from a process hydrological research site in the Black Forest Mountains, Germany. Hydrological Processes 23, 1501–1513.

Konyai, V.S., Sriboonlue, V., Trelo-Ges, V., 2009. The effect of air entry values on hysteresis of water retention curve in saline soil. American Journal of Environmental Science 5, 341–345.

Lu, N., Likos, W.J., 2004. Unsaturated Soil Mechanics. John Wiley and Sons.

Malik, R.S., Kumar, S., Malik, R.K., 1989. Maximal capillary rise flux as a function of height from the water table. Soil Science Society of America Journal 148, 322–326.

Mavko, G., Mukerji, T., Dvorkin, J., 1998. The Rock Physics Handbook, first ed. Cambridge University Press.

Meakin, P., Tartakovsky, A.M., 2009. Modeling and simulation of pore-scale multiphase fluid flow and reactive transport in fractured and porous media. Reviews of Geophysics 47, 1–47.

Mindlin, R., 1949. Compliance of elastic bodies in contact. Journal of Applied Mechanics 16, 259–268.

National Instruments (2009). LabView Virtual Instrument Software V 8.6.1.

Neill, J.D., 1990. Use of electromagnetic methods for groundwater studies. in: Ward, S.H. (Ed.), Geotechnical and Environmental Geophysics. Society Exploration Geophysics, Tulsa, OK, pp. 191–218.

Nyman, J.A., Delaune, R.D., Patrick, W.H., 1990. Wetland soil formation in the rapidly subsiding mississippi river deltaic plain: mineral and organic matter relationships. Estuarine, Coastal Shelf Science 31, 57–69.

Oreskes, N., Shrader-Frechette, K., Belitz, K., 2007. Verification, validation, and confirmation of numerical models in the earth sciences. Science 263, 641–646.

Parsekian, A.D., Slater, L., Giménez, D., 2012. Application of ground-penetrating radar to measure near-saturation soil water content in peat soils. Water Resources Research 48, W02533.

Prasad, M., Meissner, R., 1992. Attenuation mechanisms in sands: laboratory versus theoretical (Biot) data. Geophysics 57, 710–719.

Santamarina, J.C., Rinaldi, V.A., Fratta, D., Klein, K.A., Wang, Y.-H., Cho, G.C., Cascante, G., 2005. A survey of elastic and electromagnetic properties of near-surface coils. in: Butler, D.K. (Ed.), Near-Surface Geophysics. Society Exploration Geophysics, Tulsa, OK, pp. 71–88.

Sherlock, D.H., Evans, B.J., 2001. The development of seismic reflection sandbox modeling. AAPG Bulletin 85, 1645–1659.

Sioseis, 2011. A computer system for enhancing and manipulating marine seismic reflection and refraction data. ⟨http://sioseis.ucsd.edu/⟩, version 2011.3.16 [Accessed 15 Dec. 2011].

Sloan, S.D., Tsoflias, G.P., Steeples, D.W., 2007. Shallow seismic AVO variations related to partial water saturation during a pumping test. Geophysical Research Letters, 34.

Smolkin, D., 2011. Laboratory Scale Seismic Analysis of a Spatially Variable Hydrological Surface in Unconfined, Unconsolidated Sand, M.Sc. Thesis, Geology & Geophysics. Louisiana State University, 95 pp.

Stockwell, J.W., 1999. The CWP/SU: Seismic Unix Package. Computers & Geosciences 25, 415–419.

Socco, L.V., Strobbia, C., 2004. Surface waves method for near surface characterization-tutorial. Near-Surface Geophysics 2, 165–185.

Velea, D., Shields, F.D., Sabatier, J.M., 2000. Elastic wave velocities in partially saturated Ottawa sand: experimental results and modeling. Soil Science Society of America Journal 64, 1226–1234.

Vincent, P.D., Steeples, D.W., Tsoflias, G.P., Sloan, S.D., 2005. Two approaches to noise tests. SEG Technical Program Expanded Abstracts 24, 1180–1183.

Wentworth, C.K., 1922. A scale of grade and class terms for clastic sediments. Journal of the Geological Society of London 30, 377–392.

Zhody, A.A.R., Eaton, G.P., Mabey, D.R., 1974. Application of surface geophysics to ground–water investigations. Techniques of Water-Resources Investigations of the United States Geological Survey, 116.

---

[1] *Deceased.*